Available online at www.sciencedirect.com
ScienceDirect
Journal of Catalysis 255 (2008) 335–342
JOURNAL OF CATALYSIS
www.elsevier.com/locate/jcat

Excellent catalytic properties over nanocomposite catalysts for selective hydrogenation of halonitrobenzenes

Minghui Liang, Xiaodong Wang, Hongquan Liu, Haichao Liu, Yuan Wang *

Beijing National Laboratory for Molecular Sciences, State Key Laboratory for Structural Chemistry of Unstable and Stable Species, College of Chemistry & Molecular Engineering, Peking University, Beijing 100871, PR China

Received 31 October 2007; revised 25 February 2008; accepted 27 February 2008

Abstract

A partially reduced Pt/γ-Fe_2O_3 magnetic nanocomposite catalyst (Pt/γ-Fe_2O_3-PR) exhibited excellent catalytic properties in the selective hydrogenation of 2,4-dinitrochlorobenzene and iodonitrobenzenes. The selectivity to 4-chloro-*m*-phenylenediamine (4-CPDA), *meta*-iodoaniline (*m*-IAN), and *para*-iodoaniline (*p*-IAN) reached 99.9%, 99.8%, and 99.4%, respectively, at complete conversion of the substrates. The hydrodehalogenation of 4-CPDA and IANs was fully suppressed for the first time over Pt/γ-Fe_2O_3-PR. It was found that CO chemisorption on the Pt nanoparticles deposited on the partially reduced γ-Fe_2O_3 and Fe_3O_4 nanoparticles was very weak, implying a weak tendency of the electronic back-donation from the Pt nanoparticles to the π^* antibonding orbitals of the adsorbed molecules. We believe that this is a cause of the superior selectivity to the haloanilines in the hydrogenation reactions of interest over the Pt/γ-Fe_2O_3-PR catalyst.

Keywords: Platinum nanoclusters; Magnetic nanocomposite catalyst; Hydrogenation; 4-Chloro-*m*-phenylenediamine; Iodoaniline

1. Introduction

Aromatic haloamines are important organic intermediates in the synthesis of organic dyes, perfumes, herbicides, pesticides, preservatives, plant growth regulators, medicines, and light-sensitive or nonlinear optical materials [1,2]. These widely applied organic amines are produced mainly by the selective hydrogenation of the corresponding aromatic halonitro compounds over metal catalysts, such as noble metals and Raney nickel; however, hydrodehalogenation of the aromatic haloamine products often occurs over most metal catalysts, including platinum, palladium, rhodium, nickel, and copper chromite, because hydrogenolysis of the carbon–halogen bond is enhanced by amino substitution in the aromatic rings [3].

Recently, we reported that Ru/SnO_2 [4] and magnetic Pt/γ-Fe_2O_3 [5] nanocomposite catalysts exhibited excellent catalytic activity and selectivity to *ortho*-chloroaniline (*o*-CAN) in the hydrogenation of *ortho*-chloronitrobenzene (*o*-CNB). Over the activated Pt/γ-Fe_2O_3 nanocomposite catalyst, the hydrodechlorination of *o*-CAN was completely inhibited. Ag/SiO_2 [6] and Au/SiO_2 [7] also have been reported to exhibit very excellent selectivity to CAN in the hydrogenation of CNB, although further improvements in the catalytic activity of Ag/SiO_2 and Au/SiO_2 seem to be necessary before these catalysts can be used in the industrial production of CAN.

In the field of selective hydrogenation of halonitrobenzenes, successive research efforts [8–12] have been made for the selective hydrogenation of chlorine-substituted mononitrobenzenes, whereas reports on the selective hydrogenation of chlorine-substituted dinitrobenzenes or iodine-substituted nitrobenzenes have been very limited [13–16]. It is well known that the Cl–C bond in chlorophenylenediamines (CPDAs) and the I–C bond in iodoanilines (IANs) are more susceptible to hydrogenolysis than the Cl–C bond in chloroanilines (CANs). This is due to the facts that the second amino group as an electron-donating group further promotes the hydrogenolysis of the Cl–C bond in CPDAs [3,13,14], and that the large atomic diameter as well as low electronegativity of iodine results in the much weaker I–C bond relative to the Cl–C bond [14–16].

* Corresponding author. Fax: +86 10 6276 5769.
E-mail address: wangy@pku.edu.cn (Y. Wang).

0021-9517/$ – see front matter
doi:10.1016/j.jcat.2008.02.025

Winans reported that in the hydrogenation of 2,4-dinitrochlorobenzene (2,4-DNCB) and *o*-iodonitrobenzene (*o*-INB) over a nickel catalyst, 91% of 2,4-DNCB was transformed into the dechlorinated byproduct *m*-phenylenediamine (*m*-PDA), and the yield of o-iodoaniline (*o*-IAN) was only 23% [14]. Krishnan determined that the yield of 4-CPDA in the hydrogenation of 2,4-DNCB over a Pt/C catalyst was about 89%, and the byproducts were mainly the dechlorinated compounds [17]. Earlier strategies for minimizing such hydrodehalogenation in the hydrogenation of DNCBs and INBs involved mainly either alloying the catalytic metals or introducing dehalogenation inhibitors into the reaction media. For example, Maleski and Mullins reported that over Raney nickel catalysts alloyed with Al, Mo, or Co, the highest yield of 4-CPDA in the hydrogenation of 2,4-DNCB could be improved to ca. 92.5% [18]. For this reaction, Baumeister et al. decreased the yield of the dechlorinated byproducts to 3% over Raney nickel by introducing formamidine acetate as an inhibitor [13]. It also has been reported that in the hydrogenation of *m*-INB, introducing phosphorous acid as an inhibitor into the reaction system could increase the yield of *m*-IAN to 93% over a Pt/C catalyst [16]. But these methods still cannot provide complete suppression of the hydrodehalogenation of aromatic haloaniline products. Moreover, addition of the dehalogenation inhibitors into the reaction systems often restrains the hydrogenation rates of halonitrobenzenes and leads to difficulty in separating the products.

Consequently, it remains a challenge to completely inhibit the hydrodehalogenation of CPDAs and IANs in the hydrogenation of DNCBs and INBs and maintain the high catalytic hydrogenation rates of the corresponding halonitrobenzenes over noble metal catalysts. The production of CPDAs and IANs of high purity by efficient hydrogenation of the corresponding halonitrobenzenes is not only of commercial interest, but also of significance in fundamental scientific research. In this paper, we report the excellent catalytic properties of a partially reduced Pt/γ-Fe_2O_3 nanocomposite catalyst (Pt/γ-Fe_2O_3-PR) for the selective hydrogenation of 2,4-DNCB and INBs. Over this catalyst, the reactions of interest could be accomplished with high rates and superior selectivities to the target products 4-CPDA, *m*-IAN, and *p*-IAN. The hydrodehalogenation of CPDA and IANs was fully inhibited for the first time.

The perfect selectivity to haloanilines over our Pt/γ-Fe_2O_3-PR nanocomposite catalyst in the hydrogenation of halonitrobenzenes, including CNB [5], bromonitrobenzene (BNB) [19], DNCB, and INB reflects some specific interactions between the nanoparticles of Pt and iron oxides in Pt/γ-Fe_2O_3-PR.

It was found for the first time that CO could hardly be chemisorbed on the Pt nanoparticles deposited on the partially reduced γ-Fe_2O_3 nanoparticles under our measurement conditions, implying a weak tendency of the d-electron backdonation from the Pt nanoparticles to the π^* antibonding orbitals of the adsorbed molecules. We believe that this characteristic is a reason for the superior selectivity to the haloanilines in the hydrogenation reactions of interest over the partially reduced Pt/γ-Fe_2O_3 catalyst (Pt/γ-Fe_2O_3-PR).

2. Experimental

2.1. Reagents

Hydrogen (99.999%) was supplied by Beijing Gases Company. Pt/C (5 wt%) was purchased from ACROS. 2,4-DNCB (ACROS, 99%), 2-chloro-5-nitroaniline (ACROS, 99%), 4-chloro-3-nitroaniline (ACROS, 97%), 4-CPDA (TCI, 98%), *m*-INB (Alfa, 99%), *p*-INB (Alfa, 98%), *m*-IAN (Alfa, 98%), *p*-IAN (Alfa, 99%), biphenyl (Alfa, 99%) and methanol (Fisher, HPLC grade, 99.9%) were used without further purification. All other reagents used in this work were of analytical grade.

2.2. Catalyst preparation

The Pt/γ-Fe_2O_3 nanocomposite catalyst was prepared as described previously [5], with some modifications. In a typical experiment, an aqueous solution of ammonia (10%) was added dropwise to a solution of $FeCl_3$ in 100 ml of water (4%) to adjust the pH to about 7.5, producing a precipitate that was separated by a filter, washed with water, and peptized in 30 ml of aqueous solution of $FeCl_3$ (1.2%), resulting in a transparent colloidal solution of ferric hydroxide. The ferric hydroxide colloidal solution was mixed with 20% volume of ethylene glycol and a colloidal solution of Pt nanoclusters ($d_{av} = 2.2$ nm) in ethylene glycol [20] at the required ratio. The mixture was heated in a Teflon-lined autoclave at 353 K for 3 days to produce a magnetic precipitate, which was separated by an applied magnetic field, washed with water and methanol, and dried at 353 K in air, giving a brownish-red solid of Pt/γ-Fe_2O_3 (1 wt% Pt).

To study the IR spectra of CO adsorbed on the catalysts, four samples were prepared involving Pt/γ-Fe_2O_3-PR, Pt/γ-Fe_2O_3-PR-O, Pt/γ-Fe_2O_3-R, and Pt/Fe_3O_4-imp. Pt/γ-Fe_2O_3-PR (the activated catalyst) was obtained by reducing fresh Pt/γ-Fe_2O_3 (1 wt% Pt) in methanol at 303 K with hydrogen under atmospheric pressure for 45 min and drying under vacuum. Pt/γ-Fe_2O_3-PR-O was obtained through the oxidation of Pt/γ-Fe_2O_3-PR at 353 K for 2 days in air. Pt/γ-Fe_2O_3-R was prepared by reducing fresh Pt/γ-Fe_2O_3 under flowing hydrogen at 373 K for 30 min in a tubular furnace. Pt/Fe_3O_4-imp (Pt: 3 wt%) was prepared by the conventional impregnation method with $H_2PtCl_6{\cdot}6H_2O$ and γ-Fe_2O_3 as the initial materials.

2.3. Catalytic reactions

Hydrogenation of 2,4-DNCB, *m*-INB, or *p*-INB was carried out in a 50-ml reactor under magnetic stirring at 303 K and atmospheric pressure. Before the reaction, air in the system was replaced by hydrogen 15 times, and the catalyst, Pt/γ-Fe_2O_3 (1 wt%, 0.05 g) or Pt/C (5 wt%, 0.01 g), dispersed in 10 ml methanol, was activated under hydrogen for 30 min. Then a methanol solution of 2,4-DNCB, *m*-INB, or *p*-INB was added to the reactor to start the reaction. The hydrogen uptake was monitored by a constant pressure gas burette. The products were identified by GC-MS coupling (Perkin-XL) and quantitatively analyzed by gas chromatography (Shimadzu GC-2010),

using a flame ionization detector and a capillary column Rtx-5 MS (∅0.25 mm × 60 m). Biphenyl as an internal standard substance was added into the samples for GC measurement rather than into the reaction system, to avoid its influence on the reaction. The semiquantitative analysis of trace amounts (<0.1%) of aniline (AN) or *m*-PDA in the reaction mixture was conducted by comparing the peak area of AN or *m*-PDA in the GC analyses with that of a standard solution with an AN or *m*-PDA content of 0.1%.

2.4. Characterization of the catalyst

2.4.1. IR-CO probe characterization of the catalysts

Five samples were tested involving fresh Pt/γ-Fe_2O_3 (25 mg), Pt/γ-Fe_2O_3-PR (25 mg), Pt/γ-Fe_2O_3-PR-O (25 mg), Pt/γ-Fe_2O_3-R (25 mg), and Pt/Fe_3O_4-imp (15 mg). In a typical experiment, the Pt/γ-Fe_2O_3 catalyst was ground under air and pressed into a self-supporting wafer with a diameter of 1.5 cm, which was treated in the IR cell under vacuum of $1 \sim 3 \times 10^{-5}$ Torr at 373 K for 2 h to remove adsorbed water and impurities on the sample. After the sample was cooled to 303 K, 5 kPa of CO was charged into the IR cell to achieve the chemisorption equilibrium. The gaseous CO was removed by evacuation, and the spectrum of CO adsorbed on the catalyst was recorded on a FTIR spectrometer (Tensor 27, Bruker) with a resolution of 4 cm^{-1}. The IR spectrum of the sample before contacting CO was used as a subtraction background.

In another experiment, a self-supporting wafer of the Pt/γ-Fe_2O_3-PR catalyst (25 mg) was first treated under flowing hydrogen at 323 K for 2 h, and then heated at 573 K in vacuum for 3 h in the IR cell. IR-CO probe measurements on this sample were conducted in the same manner and conditions as applied in the typical experiment.

2.4.2. CO chemisorption on the catalysts

In the chemisorption experiments on the fresh and partially reduced Pt/γ-Fe_2O_3 catalysts, the CO/Pt ratio was determined on an ASAP 2010C. In the analysis of the reduced sample, 0.05 g of Pt/γ-Fe_2O_3 (3 wt%) was loaded into a U-type tube and treated in the following steps: evacuation at 308 K for 0.5 h and then at 473 K for 1 h, reduction by flowing hydrogen at 383 K for 1 h, and evacuation at 573 K for 2 h and at 308 K for 0.5 h. The CO adsorption was measured at 308 K and at 4–25 kPa of CO. The fresh catalyst was treated and analyzed as described previously, except for the hydrogen reduction process.

2.4.3. XPS measurement of the catalysts

XPS measurements were carried out with an Axis Ultra photoelectron spectrometer using an Al$K\alpha$ (1486.7 eV) X-ray source, with the pressure of the measuring chamber set at 5×10^{-9} Torr. The binding energy scales for the samples were referenced by setting the C 1s binding energy of contamination carbon to 284.8 eV. The Pt/γ-Fe_2O_3-PR catalyst for the XPS measurement was prepared by reducing fresh Pt/γ-Fe_2O_3 (Pt: 1 wt%) with hydrogen at 303 K for 1 h in the pretreatment chamber of the XPS spectrometer. The sample was moved to the analysis chamber after the pretreatment chamber was flushed with argon and evacuated.

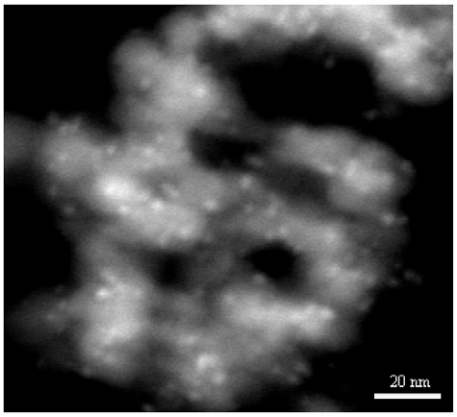

Fig. 1. STEM image of Pt nanoparticles dispersed on the iron oxide support. The small bright spots were Pt nanoparticles which deposited on the nanoparticles of iron oxide (see Ref. [5]).

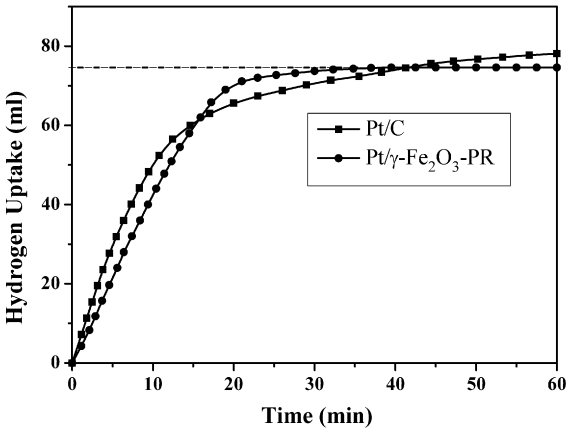

Fig. 2. Cumulative hydrogen uptake of 2,4-DNCB hydrogenation over Pt/γ-Fe_2O_3-PR and Pt/C catalysts. Reaction conditions: temperature, 303 K; hydrogen pressure, 0.1 MPa; substrate, 0.5 mmol; solvent, 20 ml methanol; loading of Pt, 0.5 mg.

3. Results and discussion

The Pt/γ-Fe_2O_3 (1 wt%) nanocomposite catalyst used in this work had a specific surface area of 79 m^2/g. The Pt nanoclusters, with an average diameter of 2.2 nm as measured by scanning transmission electron microscopy (STEM), were well dispersed in the matrix composed of γ-Fe_2O_3 nanoparticles, as shown in Fig. 1. During activation of the Pt/γ-Fe_2O_3 catalyst in methanol under 0.1 MPa of hydrogen pressure at 303 K, a color change from brownish-red to black was observed. XRD measurements revealed that γ-Fe_2O_3 nanoparticles in the catalyst were partially reduced by hydrogen, due to the catalytic function of the attached Pt nanoclusters [19]; therefore, the actual catalyst in the present catalytic reactions was the partially reduced Pt/γ-Fe_2O_3 nanocomposite (Pt/γ-Fe_2O_3-PR).

Fig. 2 shows the cumulative hydrogen uptake curves in the hydrogenation of 2,4-DNCB over Pt/γ-Fe_2O_3-PR and Pt/C catalysts. Over the Pt/γ-Fe_2O_3-PR nanocomposite catalyst, the

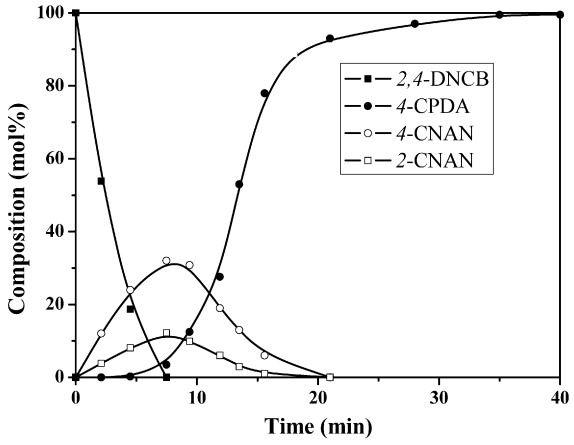

Fig. 3. Composition of the reaction mixture of 2,4-DNCB hydrogenation over the Pt/γ-Fe_2O_3-PR catalyst as a function of time. Reaction conditions were similar to those in Fig. 2.

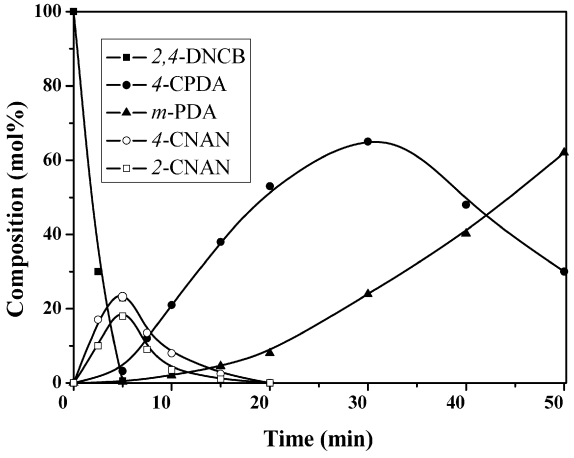

Fig. 4. Composition of the reaction mixture of 2,4-DNCB hydrogenation over the Pt/C catalyst as a function of time. Reaction conditions were similar to those in Fig. 2.

hydrogen uptake reached the theoretical amount for the complete transformation of 2,4-DNCB into 4-CPDA within 35 min. Subsequently, no further increase in the hydrogen uptake was detected during the extended reaction time. Quite different features of the hydrogen uptake curve were observed over the Pt/C catalyst, which was characterized by a fast initial rate of hydrogen consumption, with a further increase in hydrogen uptake after the stoichiometric hydrogen for producing 4-CPDA was consumed. A similar hydrogen uptake discrepancy over the Pt/γ-Fe_2O_3-PR and Pt/C catalysts was observed in the hydrogenation of *m*-INB and *p*-INB.

The reaction pathways in the hydrogenation of halonitrobenzenes have been intensively investigated [3,4,19]. The evolution of the detectable reaction compounds measured by GC during the hydrogenation of 2,4-DNCB over Pt/γ-Fe_2O_3-PR and Pt/C is characterized in Figs. 3 and 4. It can be seen from Fig. 3 that over the Pt/γ-Fe_2O_3-PR catalyst, the yield of the desired product 4-CPDA increased monotonously, reaching 99.9% when the reaction was accomplished. The content of dechlorinated byproduct *m*-PDA in the final products was <0.1%. Extending the reaction time to 5 h caused no detectable increase in the *m*-PDA content. On the contrary, as shown in Fig. 4, over the Pt/C catalyst, the highest yield of 4-CPDA in the entire hydrogenation process was only 65%. When the reaction was conducted for 50 min, the yield of 4-CPDA decreased to 30%, and the content of *m*-PDA in the reaction mixture increased to 62%.

Table 1
Catalytic properties of Pt/γ-Fe_2O_3-PR and Pt/C for the hydrogenation of *m*-INB[a]

Catalyst	Reaction time (min)	Initial H_2 uptake rate[b] ($\times 10^{-2}$)	Yield of products (mol%)	
			m-IAN	AN
Pt/C[c]	75		46	23
Pt/C	160[d]	66	42	51
Pt/C	300		35	58
Pt/γ-Fe_2O_3-PR	38[d]	30	99.8	0.2
Pt/γ-Fe_2O_3-PR	300		99.8	0.2

[a] Reaction conditions: temperature, 303 K; hydrogen pressure, 0.1 MPa; substrate, 0.375 mmol; solvent, 30 ml methanol; loading of Pt, 0.5 mg.
[b] $mol_{Hydrogen}/(mol_{Pt}\ s)$.
[c] The reaction was not complete.
[d] Reaction time for the complete conversion of the substrate and all intermediates.

The appearance, increased and decreased content, and disappearance of the 4-chloro-3-nitroaniline (4-CNAN) and 2-chloro-5-nitroaniline (2-CNAN) intermediates also were observed over both the Pt/γ-Fe_2O_3-PR and Pt/C catalysts. In addition, the formation of the coupling intermediates, such as 3,3′-diaminoazo- and azoxychlorobenzenes, was detected in the reaction process by GC-MS analysis. The further increase in yield of 4-CPDA over the Pt/γ-Fe_2O_3-PR catalyst after the complete exhaustion of the substrate as well as 4-CNAN and 2-CNAN intermediates should be derived from the transformation of the coupling intermediates.

The results for *m*-INB hydrogenation over the Pt/γ-Fe_2O_3-PR and Pt/C catalysts are summarized in Table 1. Over the Pt/C catalyst, the reaction time for the complete conversion of the substrate and all of the intermediates was 160 min under the specified conditions. When the substrate and intermediate products were exhausted, the selectivity to *m*-IAN, AN, and other byproducts was 42%, 51%, and 7%, respectively. The highest yield of *m*-IAN obtained over the Pt/C catalyst was only 46% during the entire course of the reaction. But excellent catalytic properties for the hydrogenation of *m*-INB were achieved over the Pt/γ-Fe_2O_3-PR nanocomposite catalyst. Over this catalyst, the reaction time for the complete conversion of the substrate and all of the intermediates was only 38 min, with an average product formation rate of 6.4×10^{-2} $mol_{m\text{-IAN}}/(mol_{Pt}\ s)$. Obviously the average formation rate of *m*-IAN over Pt/γ-Fe_2O_3-PR was much higher than that over the Pt/C catalyst, although the initial rate of hydrogen uptake over the Pt/C catalyst was 2.2 times that over Pt/γ-Fe_2O_3-PR. The *m*-IAN selectivity of 99.8% was obtained at complete conversion of the substrate and intermediates over Pt/γ-Fe_2O_3-PR, and the content of AN in the final products was only about 0.2%. Moreover, extending the reaction time after the exhaustion of the substrate and all intermediates caused no detectable increase in the content of the deiodination byproduct over the Pt/γ-Fe_2O_3-PR catalyst.

In the case of *p*-INB hydrogenation, the highest yield of *p*-IAN obtained over the Pt/C catalyst was 43%. When the substrate and intermediates were completely exhausted, the *p*-IAN yield decreased to 33%. Sequentially extending the reaction time under the reaction conditions would cause further deiodination of *p*-IAN. When the reaction was conducted for 300 min, the content of the desired product, *p*-IAN, was only 9% over the Pt/C catalyst, whereas the content of AN in the reaction mixture increased to 83% (Table 2). In contrast, over Pt/γ-Fe_2O_3-PR, the selectivity to *p*-IAN was as high as 99.4%. This high selectivity could be maintained even when the reaction time was extended by several hours after *p*-INB was exhausted. Similar to the case of *m*-INB hydrogenation, although the initial rate of hydrogen uptake over the Pt/C catalyst was 2.5 times that over Pt/γ-Fe_2O_3-PR, the average formation rate of *p*-IAN was much higher over Pt/γ-Fe_2O_3-PR than over the Pt/C catalyst. This finding may be related to the polarization effect of the iron cations in the catalyst surface on the –NO groups in iodonitrosobenzene [19].

Reaction conditions have been reported to have certain effects on the hydrogenation rate and catalytic selectivity in the hydrogenation of CNBs over some supported metal catalysts [16,21]. In the present work, we investigated the influence of reaction temperature and hydrogen pressure on the hydrogenation of *p*-INB over the Pt/γ-Fe_2O_3-PR catalyst; the results, summarized in Table 3, show that the hydrogenation rate of *p*-INB over the Pt/γ-Fe_2O_3-PR catalyst reached a maximum value with increasing reaction temperature, with the optimum temperature about 313 K. At temperatures above 323 K, the hydrogenation rate decreased significantly, and the selectivity to *p*-IAN declined slightly. The reaction rate was enhanced 12-fold with increasing hydrogen pressure from 0.1 to 8.0 MPa; an increased hydrogen pressure also had a positive effect on catalyst selectivity.

We also investigated the stability of the Pt/γ-Fe_2O_3-PR catalyst at 293 K and 3.0 MPa of hydrogen. In the hydrogenation of *m*-INB with a substrate/Pt molar ratio of 50,000 and a substrate concentration of 0.5 M, a selectivity to *m*-IAN of 99.9% and an average catalytic activity of 1.85 $mol_{m\text{-INB}}/(mol_{Pt}\,s)$ were obtained over Pt/γ-Fe_2O_3-PR. Moreover, the recovered catalyst could be reused for recycling experiments, and a total turnover number (TON) of >100,000 over Pt/γ-Fe_2O_3-PR for *m*-INB hydrogenation could be achieved with no detectable loss of the superior selectivity to *m*-IAN. These results suggest that the Pt/γ-Fe_2O_3-PR catalyst is very stable and suitable for practical applications.

To verify the suppression capability of the partially reduced γ-Fe_2O_3 nanoparticles in Pt/γ-Fe_2O_3-PR for the hydrodehalogenation of haloanilines over the Pt nanoparticles, we compared the hydrogenolysis activity of carbon-halogen bonds in 4-CPDA and *p*-IAN over the Pt/γ-Fe_2O_3-PR, fresh Pt/γ-Fe_2O_3, and Pt/C catalysts. As shown in Table 4, over the Pt/C catalyst, in a 5-h hydrogenolysis of *p*-IAN, 97% of *p*-IAN was consumed and converted into 93% of AN and 4% of other products. In contrast, no dehalogenated products were detected over

Table 2
Catalytic properties of Pt/γ-Fe_2O_3-PR and Pt/C for the hydrogenation of *p*-INB[a]

Catalyst	Reaction time (min)	Initial H_2 uptake rate[b] ($\times10^{-2}$)	Yield of products (mol%)	
			p-IAN	AN
Pt/C[c]	45		43	25
Pt/C	90[d]	90	33	59
Pt/C	300		9	83
Pt/γ-Fe_2O_3-PR	36[d]	36	99.4	0.6
Pt/γ-Fe_2O_3-PR	300		99.4	0.6

[a] Reaction conditions are similar to those in Table 1.
[b] $mol_{Hydrogen}/(mol_{Pt}\,s)$.
[c] The reaction was not complete.
[d] Reaction time for the complete conversion of the substrate and all intermediates.

Table 3
Effects of reaction temperature and hydrogen pressure on the hydrogenation of *p*-INB over the Pt/γ-Fe_2O_3-PR catalyst[a]

Reaction temperature (K)	P_{H_2} (MPa)	Loading of Pt (mg)	Reaction rate[b] ($\times10^{-2}$)	Yield of products (mol%)	
				p-IAN	AN
303	0.1	0.5	6.8	99.4	0.6
313	0.1	0.5	8.1	99.4	0.6
323	0.1	0.5	6.6	99.3	0.7
333	0.1	0.5	3.4	99.2	0.8
303	1.0	0.1	44	99.5	0.5
303	2.0	0.1	64	99.6	0.4
303	4.0	0.1	76	99.7	0.3
303	8.0	0.1	81	99.8	0.2

[a] Reaction conditions: *p*-INB, 0.375 mmol; solvent, 30 ml methanol.
[b] Average rate, $mol_{p\text{-INB}}/(mol_{Pt}\,s)$.

Table 4
Hydrodehalogenation of 4-CPDA and *p*-IAN over the Pt-based catalysts[a]

Catalyst	Hydrodechlorination of 4-CPDA[b]			Hydrodeiodination of *p*-IAN[c]		
	Reaction time (h)	Composition (mol%)		Reaction time (h)	Composition (mol%)	
		4-CPDA	*m*-PDA		*p*-IAN	AN
Pt/γ-Fe_2O_3[d]	1	99.7	0.3	–	–	–
Pt/γ-Fe_2O_3-PR[e]	15	>99.9	<0.1	5	>99.9	<0.1
Pt/C	–	–	–	5	3	93

[a] Reaction conditions: temperature, 303 K; hydrogen pressure, 0.1 MPa; loading of Pt, 0.5 mg.
[b] 0.50 mmol of 4-CPDA in 20 ml methanol.
[c] 0.375 mmol of *p*-IAN in 30 ml methanol.
[d] Catalyst was used without the activation process.
[e] Catalyst was activated at 303 K and 0.1 MPa of hydrogen pressure for 30 min before used for the reaction.

Pt/γ-Fe_2O_3-PR during the reaction process of either *p*-IAN or 4-CPDA, further confirming that the hydrodehalogenation of the haloanilines was fully inhibited over Pt/γ-Fe_2O_3-PR. The trace of *m*-PDA or AN produced in the hydrogenation of 2,4-DNCB or INBs over this catalyst was derived from other hydrogenolysis processes [19]. Moreover, over a Pt/Fe_3O_4 catalyst (Pt: 3 wt%) prepared by the impregnation method, the same selectivity to 4-CPDA in the hydrogenation of 2,4-DNCB was achieved, and the hydrodehalogenation reaction of the product was also completely suppressed. But over fresh Pt/γ-Fe_2O_3 without activation with H_2 before the reaction, a slow dehalogenation process was observed in the hydrogenolysis of 4-CPDA. These experimental findings indicate that the structure of the actual catalytic site that exhibits excellent selectivity to the aromatic haloamines is characterized by Pt nanoparticles deposited on the partially reduced γ-Fe_2O_3 or Fe_3O_4 particles.

Regarding the mechanism of the hydrodehalogenation of haloanilines over metal catalysts, most researchers agree that it involves an electrophilic attack of cleaved hydrogen on the carbon–halogen bond [22–24]. We have previously reported that the electronic back-donation from Pt nanoclusters to the aromatic ring in the produced haloanilines favors the hydrogenolysis reaction, because such a back-donation effect weakens the p–π conjugation between the halogen atom and the benzene ring [5].

To investigate the electronic back-donation effect of the Pt particles in the Pt/γ-Fe_2O_3-PR catalyst, we conducted IR-CO probe and CO chemisorption experiments on the catalysts, because the chemisorption of CO on iron oxide is negligible at room temperature [25,26]. The chemisorption of CO on the surface of Pt nanoparticles occurs mainly in a linear form [27]. The extent of electronic back-donation from the d orbitals of Pt to the $2\pi^*$ orbital of CO plays an important role in the stability of Pt–CO coordination [26]. If the extent of the back-donation from Pt particles is weakened, then the adsorption strength of CO on the Pt particles decreases, and the amount of CO chemisorbed on the Pt-based catalysts is decreased accordingly.

Fig. 5a shows the IR spectrum of CO adsorbed on the fresh Pt/γ-Fe_2O_3 catalyst. In this spectrum, a strong peak centered at 2070 cm^{-1} can be attributed to the signal of CO adsorbed on the on-top site in Pt surface, whereas a broad band in the range of 1730–1870 cm^{-1} may be ascribed to the signals of CO adsorbed on the bridge and 3-fold sites on the Pt surface [26,28]. However, the typical signals of CO adsorbed on Pt were not detected in the IR-CO probe measurements on Pt/γ-Fe_2O_3-PR (Fig. 5b), suggesting that the chemisorption of CO on the Pt nanoparticles in the Pt/γ-Fe_2O_3-PR was very weak and unstable at room temperature. The magnetic and brownish-red Pt/γ-Fe_2O_3-PR-O catalyst was prepared by the oxidation of Pt/γ-Fe_2O_3-PR in air at 353 K for 2 days. The typical signals of CO adsorbed on Pt particles were clearly detected in the IR-CO probe measurements on Pt/γ-Fe_2O_3-PR-O (Fig. 5c), confirming that CO can be stably adsorbed on the Pt/γ-Fe_2O_3 catalysts.

To avoid the possible influence of the solvent or impurities on the IR-CO probe measurements on Pt/γ-Fe_2O_3-PR, fresh Pt/γ-Fe_2O_3 was partly reduced with hydrogenation at 373 K in a tubular furnace for 30 min. The results of IR-CO probe experiments on the Pt/γ-Fe_2O_3-R sample (Fig. 5d) were identical to those on Pt/γ-Fe_2O_3-PR. In addition, the signals of CO adsorbed on the Pt particles in the Pt/Fe_3O_4 catalyst prepared by the impregnation method also were not detectable in our experiments (Fig. 5e).

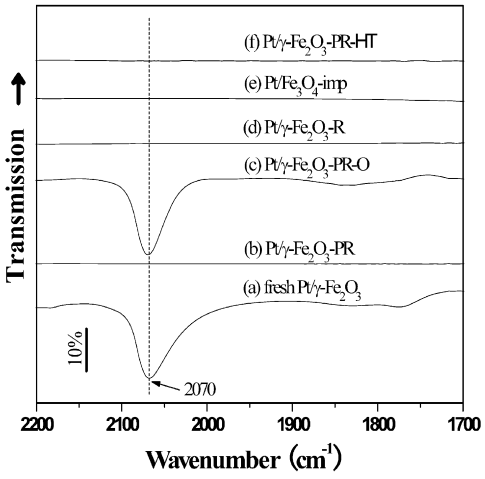

Fig. 5. Infrared spectra of CO adsorbed on (a) fresh Pt/γ-Fe_2O_3, (b) Pt/γ-Fe_2O_3-PR prepared by reducing Pt/γ-Fe_2O_3 in methanol with hydrogen at 303 K for 45 min, (c) Pt/γ-Fe_2O_3-PR-O prepared by oxidizing Pt/γ-Fe_2O_3-PR at 353 K for 2 days under air, (d) Pt/γ-Fe_2O_3-R prepared by reducing Pt/γ-Fe_2O_3 by flowing hydrogen at 373 K for 30 min, (e) Pt/Fe_3O_4-imp prepared by the impregnation method, and (f) Pt/γ-Fe_2O_3-PR-HT prepared by treating Pt/γ-Fe_2O_3-PR with hydrogen in the IR cell at 323 K and heating in vacuum at 573 K for 3 h.

To further validate the weak chemisorption of CO on Pt/γ-Fe_2O_3-PR, we measured the amounts of CO chemisorbed on the Pt nanoparticles in the Pt/γ-Fe_2O_3 and Pt/γ-Fe_2O_3-PR catalysts. For the fresh Pt/γ-Fe_2O_3 catalyst evacuated at 573 K, the CO/Pt ratio in the CO chemisorption experiment was determined to be 15.6%; in contrast, for the partially reduced catalyst Pt/γ-Fe_2O_3-PR treated under the same conditions, the measured CO/Pt ratio was as low as 0.02%. Because Pt/γ-Fe_2O_3-PR is a very active catalyst for the hydrogenation of aromatic halonitrobenzenes, and because the signals of CO adsorbed on the Pt particles in Pt/γ-Fe_2O_3 could be clearly detected in the IR-CO probe measurements, the possibility of complete encapsulation of the Pt nanoparticles by iron oxides in Pt/γ-Fe_2O_3-PR can be ruled out. The CO chemisorption results did confirm the finding that chemisorption of CO on Pt nanoparticles in the Pt/γ-Fe_2O_3-PR catalyst was very weak.

It should be mentioned that during the preparation of the Pt/γ-Fe_2O_3 catalyst and the IR samples, oxygen is adsorbed on the Pt particles, and thus a thin Pt-oxide skin possibly could form on the Pt particles. But it is known that the Pt-oxide skin can be reduced by CO at room temperature [29,30]. Moreover, Solomennikov and Davydov [31] reported that in an IR-CO probe measurement at 298 K on a Pt/Al_2O_3 catalyst that had been treated in oxygen at 673 K for 1 h, a signal at 2090 cm^{-1}, attributed to CO adsorbed on metallic Pt, was clearly detected [31]. These previous findings account for the finding of clearly detectable signals of CO adsorbed on the Pt particles in our Pt/γ-Fe_2O_3 catalyst.

To avoid the possible influence of the adsorbed oxygen or Pt-oxide skin on the IR-CO probe measurements on Pt/γ-Fe_2O_3-PR, we first treated the IR sample of Pt/γ-Fe_2O_3-PR under flowing hydrogen at 323 K for 2 h in the IR cell before the IR-CO probe measurements (see the Experimental section). The signal of CO adsorbed on the Pt particles in this sample could not be detected in our experiments, as shown in Fig. 5f.

The aforementioned results of IR-CO probe and CO chemisorption experiments definitely revealed that CO was hardly chemisorbed on the Pt nanoparticles in the Pt/γ-Fe_2O_3-PR and Pt/Fe_3O_4 catalysts under the measurement conditions. Thus suggests a very weak tendency of electronic back-donation from Pt nanoparticles in both catalysts to the adsorbed molecules. This weak tendency is obviously related to the structures of the iron oxide particles. γ-Fe_2O_3 and Fe_3O_4 have very similar cubic inverse spinel crystal structures, in which the oxygen anions (O^{2-}) form a closely packed face-centered cubic (fcc) sublattice with iron cations located in interstitial sites. In γ-Fe_2O_3, all of the iron cations are Fe^{3+}, whereas in Fe_3O_4, there are two different kinds of cation sites: tetrahedrally coordinated sites occupied by Fe^{3+} and octahedrally coordinated sites occupied by Fe^{3+} and Fe^{2+} ions in equal numbers. The Fe^{2+} cation can be considered to be Fe^{3+} plus an "extra" electron, hopping freely between the octahedral sites above the Verwey transition temperature [32].

It is known that γ-Fe_2O_3 can be reduced to Fe_3O_4 with hydrogen at about 250 °C [33]. However, as mentioned above, by virtue of the catalytic function of the Pt nanoparticles, γ-Fe_2O_3 nanoparticles in the Pt/γ-Fe_2O_3 nanocomposite were partially reduced by H_2 during the activation process at room temperature; that is, part of the Fe^{3+} cations in the Pt/γ-Fe_2O_3 nanocomposite were reduced to Fe^{2+} cations during the mild activation process. XRD studies have shown that the crystalline structure of the partially reduced γ-Fe_2O_3 nanoparticles is quite close to that of Fe_3O_4 [19]. Because the catalytic reduction of the γ-Fe_2O_3 nanoparticles should start on their surfaces, it is reasonable to deduce that the surface structure of the partially reduced γ-Fe_2O_3 nanoparticles resembles that of Fe_3O_4 particles.

The (111) surface structure of Fe_3O_4 has been intensively investigated [25,34–39]. Under oxidation conditions at high temperature, the exposed surface of Fe_3O_4(111) is terminated with oxygen atoms [36–38]; however, under more reducing conditions (i.e., annealing in vacuum without oxygen), the surface of Fe_3O_4(111) is terminated by iron cations [39]. It has been shown that Fe_3O_4(111) surface is terminated by 1/2 ML of iron, with the outermost 1/4 ML consisting of octahedral Fe^{2+} cations situated above 1/4 ML of tetrahedral Fe^{3+} ions [25]. We believe that during the partial reduction of γ-Fe_2O_3 nanoparticles in the Pt/γ-Fe_2O_3 by H_2, catalyzed by the deposited Pt nanoparticles, some of the surface O^{2-} anions in the γ-Fe_2O_3 nanoparticles will be removed by the formation of H_2O, and the Pt nanoparticles will directly contact the outermost layer of iron cations. The positive electric fields of these cations or the electron transfer from Pt nanoparticles to the cations may decrease the electronic back-donation from the d orbitals of the Pt nanoparticles to the π^* anti-orbitals of the adsorbed molecules.

XPS measurements were conducted on the Pt/γ-Fe_2O_3-PR catalyst and Pt nanoparticles with the same particle size protected by poly(*N*-vinyl-2-pyrrolidone) (PVP). The PVP-protected Pt particles were prepared by adding the colloidal solution of Pt nanoclusters applied in the catalyst preparation to an ethanol solution containing PVP. The colloidal solution thus obtained was stirred in a hydrogen atmosphere at room temperature for 1 h, after which acetone was added to the colloidal solution to form a precipitate of the PVP-protected Pt nanoparticles (PVP/Pt weight ratio = 9). The binding energy of the Pt $4f_{7/2}$ core-level in Pt/γ-Fe_2O_3-PR had a value of 71.3 eV, 0.5 eV higher than that of the Pt particles protected by PVP (70.8 eV). This provides evidence of an electron transfer from the Pt nanoparticles to iron cations or the iron oxide particles in Pt/γ-Fe_2O_3-PR.

Based on the foregoing results of hydrodehalogenation of haloanilines and the adsorptive behavior of CO on the different catalysts, a close relationship between the CO adsorption properties and the hydrodehalogenation activity over the catalysts can be inferred. The fresh Pt/γ-Fe_2O_3 catalyst on which CO can be stably adsorbed exhibited catalytic activity for the dechlorination of 4-CPDA. In contrast, Pt/γ-Fe_2O_3-PR, on which CO cannot be chemically adsorbed at room temperature, did not catalyze the hydrodehalogenation of haloanilines. Moreover, some other Pt-based catalysts with a strong capability to chemically adsorb CO, such as Pt/C [40], Pt/Al_2O_3 [41] and Pt/TiO_2 [42], can smoothly catalyze the hydrodehalogenation of haloanilines [19,22].

The electron feedback from Pt to haloanilines adsorbed on Pt/C, Pt/γ-Fe_2O_3, Pt/Al_2O_3, and Pt/TiO_2 would make the carbon-halogen bonds in the haloanilines more susceptible to an electrophilic attack of the adsorbed hydrogen atoms. The weak tendency of electronic back-donation from the Pt nanoparticles in Pt/γ-Fe_2O_3-PR to the π^* antibonding orbitals of adsorbed haloanilines would not obviously weaken the p–π conjugation between the halogen atom and the benzene ring. This is a key factor in the extremely high selectivity to haloanilines in the hydrogenation of halonitrobenzenes over Pt/γ-Fe_2O_3-PR.

Some iron oxides have been reported to be excellent catalysts for the H-transfer reduction of monosubstituted nitrobenzenes to corresponding anilines with hydrazine hydrate, and it has been found that azo groups in the substrates cannot be reduced by this process in the absence of metal particles [43,44]. But over the present Pt/γ-Fe_2O_3-PR catalyst, the azo intermediates in the hydrogenation of CNB, BNB, and INB could be easily reduced to the corresponding haloanilines; indicating that over this catalyst, the hydrogenation of halonitrobenzenes occurred mainly on the Pt nanoclusters deposited on the partly reduced γ-Fe_2O_3 particles. The possible contribution of the H-transfer reduction process to the reaction of interest over the Pt/γ-Fe_2O_3-PR catalyst remains an open question.

4. Conclusion

The Pt/γ-Fe_2O_3-PR nanocomposite catalyst exhibited very excellent catalytic properties for the selective hydrogenation of 2,4-DNCB, *m*-INB, and *p*-INB. The formation of 4-CPDA,

m-IAN, and *p*-IAN was much higher over the Pt/γ-Fe_2O_3-PR catalyst than over the Pt/C catalyst. The high catalytic selectivity (i.e., >99.9% to 4-CPDA, 99.4% to *m*-IAN, and 99.8% to *p*-IAN) could be readily achieved at complete conversion of the substrates. Moreover, the undesired hydrodehalogenation of 4-CPDA and IANs over the Pt/γ-Fe_2O_3-PR nanocomposite catalyst was fully suppressed for the first time. Increasing the hydrogen pressure from 0.1 to 8.0 MPa not only increased the hydrogenation rate of *p*-INB over the Pt/γ-Fe_2O_3-PR catalyst by one order of magnitude, but also increased the *p*-IAN selectivity to 99.8%. The Pt/γ-Fe_2O_3-PR catalyst also exhibited excellent stability. The total TON for *m*-INB hydrogenation exceeded 100,000 with an *m*-IAN selectivity of 99.9% at 293 K and 3.0 MPa H_2. IR-CO probe and CO chemisorption experiments revealed that CO was hardly chemisorbed on Pt nanoparticles in the Pt/γ-Fe_2O_3-PR catalyst under the experimental conditions, suggesting very week back-donation of d electrons from the Pt nanoparticles to the adsorbed molecules. This is considered to play an important role in the complete suppression of hydrodehalogenation of haloanilines in the hydrogenation of halonitrobenzenes over this catalyst.

Acknowledgments

This work was jointly supported by NSFC (grants 20573005, 50521201, 90206011, 20433010), Chinese Ministry of Science and Technology (NKBRSF 2006CB806102), and the Ministry of Education of China (RFDP). The authors thank Professor Jinglin Xie, College of Chemistry and Molecular Engineering, Peking University for his assistance with measuring the XPS data.

References

[1] J.O. Morley, J. Phys. Chem. 99 (1995) 1923.
[2] Y. Okazaki, K. Yamashita, H. Ishii, M. Sudo, M. Tsuchitani, J. Appl. Toxicol. 23 (2003) 315.
[3] X.D. Wang, M.H. Liang, J.L. Zhang, Y. Wang, Curr. Org. Chem. 11 (2007) 299.
[4] B.J. Zuo, Y. Wang, Q.L. Wang, J.L. Zhang, N.Z. Wu, L.D. Peng, L.L. Gui, X.D. Wang, R.M. Wang, D.P. Yu, J. Catal. 222 (2004) 493.
[5] J.L. Zhang, Y. Wang, H. Ji, Y.G. Wei, N.Z. Wu, B.J. Zuo, Q.L. Wang, J. Catal. 229 (2005) 114.
[6] Y.Y. Chen, C. Wang, H.Y. Liu, J.S. Qiu, X.H. Bao, Chem. Commun. 42 (2005) 5298.
[7] Y.Y. Chen, J.S. Qiu, X.K. Wang, J.H. Xiu, J. Catal. 242 (2006) 227.
[8] W.W. Yu, H.F. Liu, J. Mol. Catal. A 243 (2006) 120.
[9] M.H. Liu, W.Y. Yu, H.F. Liu, J. Mol. Catal. A 138 (1999) 295.
[10] X.H. Yan, J.Q. Sun, Y.W. Wang, J.F. Yang, J. Mol. Catal. A 252 (2006) 17.
[11] X.X. Han, R.X. Zhou, G.H. Lai, X.M. Zheng, React. Kinet. Catal. Lett. 83 (2004) 55.
[12] J. Wiss, A. Zilian, Org. Process Res. Dev. 7 (2003) 1059.
[13] P. Baumeister, H.U. Blaser, W. Scherrer, Stud. Surf. Sci. Catal. 59 (1991) 321.
[14] C.F. Winans, J. Am. Chem. Soc. 61 (1939) 3564.
[15] A.M. Stratz, in: J.R. Kosak (Ed.), Catalysis of Organic Reactions, Dekker, New York, 1984, p. 335.
[16] J.R. Kosak, in: W.H. Jones (Ed.), Catalysis in Organic Syntheses, Academic Press, New York, 1980, p. 107.
[17] R.M. Krishnan, US patent, 3 928 451 (1975), to Goodyear Tire and Rubber Company.
[18] R.J. Maleski, E.T. Mullins, US patent, 6 034 276 (2000), to Eastman Chemical Company.
[19] X.D. Wang, M.H. Liang, H.Q. Liu, Y. Wang, J. Mol. Catal. A 273 (2007) 160.
[20] Y. Wang, J.W. Ren, K. Deng, L.L. Gui, Y.Q. Tang, Chem. Mater. 12 (2000) 1622.
[21] X.X. Han, R.X. Zhou, G.H. Lai, X.M. Zheng, Catal. Today 93–95 (2004) 433.
[22] B. Coq, A. Tajani, R. Dutartre, F. Figuéras, J. Mol. Catal. 79 (1993) 253.
[23] C. Menini, C. Park, E. Shin, G. Tavoularis, M. Keane, Catal. Today 62 (2000) 355.
[24] S. Chon, D. Allen, AIChE J. 37 (1991) 1730.
[25] C. Lemire, R. Meyer, V.E. Henrich, S. Shaikhutdinov, H.J. Freund, Surf. Sci. 572 (2004) 103.
[26] K.I. Hadjiivanov, G.N. Vayssilov, Adv. Catal. 47 (2002) 307.
[27] Y. Wang, N. Toshima, J. Phys. Chem. B 101 (1997) 5301.
[28] K. Mikita, M. Nakamura, N. Hoshi, Langmuir 23 (2007) 9092.
[29] I. Nakai, H. Kondoh, K. Amemiya, M. Nagasaka, A. Nambu, T. Shimada, T. Ohta, J. Chem. Phys. 121 (2004) 5035.
[30] P.V. McKinney, J. Am. Chem. Soc. 56 (1934) 2577.
[31] A.A. Solomennikov, A.A. Davydov, Kinet. Katal. 25 (1984) 334.
[32] Z. Szotek, W.M. Temmerman, A. Svane, L. Petit, G.M. Stocks, H. Winter, Phys. Rev. B 68 (2003) 054415.
[33] L.S. Chen, G.L. Lu, J. Mater. Sci. 34 (1999) 4193.
[34] D.M. Huang, D.B. Cao, Y.W. Li, H.J. Jiao, J. Phys. Chem. B 110 (2006) 13920.
[35] S. Murphy, A. Cazacu, N. Berdunov, I.V. Shvets, Y.M. Mukovskii, J. Magn. Magn. Mater. 290–291 (2005) 201.
[36] Y.S. Dedkov, M. Fonin, D.V. Vyalikh, J.O. Hauch, S.L. Molodtsov, U. Rüdiger, G. Güntherodt, Phys. Rev. B 70 (2004) 073405.
[37] N. Berdunov, S. Murphy, G. Mariotto, I.V. Shvets, Phys. Rev. Lett. 93 (2004) 057201.
[38] N. Berdunov, S. Murphy, G. Mariotto, I.V. Shvets, Y.M. Mykovskiy, J. Appl. Phys. 95 (2004) 6891.
[39] S.K. Shaikhutdinov, M. Ritter, X.G. Wang, H. Over, W. Weiss, Phys. Rev. B 60 (1999) 11062.
[40] L.B. Okhlopkova, A.S. Lisitsyn, V.A. Likholobov, M. Gurrath, H.P. Boehm, Appl. Catal. A 204 (2000) 229.
[41] Q. Xin, J.H. Hu, X.X. Guo, Chin. J. Catal. 6 (1980) 138.
[42] F. Coloma, J.M. Coronado, C.H. Rochester, J.A. Anderson, Catal. Lett. 51 (1998) 155.
[43] M. Lauwiner, P. Rys, J. Wissmann, Appl. Catal. A 172 (1998) 141.
[44] M. Benz, A.M. Kraan, R. Prins, Appl. Catal. A 172 (1998) 149.